Preprints of the 19th World Congress
The International Federation of Automatic Control
Cape Town, South Africa. August 24-29, 2014

PET Image Reconstruction Based on a Constrained Filter ⋆

Hongxia Wang * **Xin Chen** * **Li Yu** *

* *Department of Automation, Zhejiang University of Technology, Hangzhou, 310023, P. R. China (e-mail: whx1123@126.com).*

Abstract: The paper aims to propose an algorithm for PET(positron emission tomography) image reconstruction. Different from the algorithms designed to satisfy a single performance index in most cases, our algorithm inherently involves for two objects. Due to that the information upon noises is utilized fully, our algorithm provides a better reconstructed results than the one for the a single index when one obtains only some information on noises but does not know whether the statistics matches the noise level well in advance. The conclusion is also supported by the numerical experiments.

Keywords: Kalman filtering, H_∞ filtering, PET, image reconstruction.

1. INTRODUCTION

PET is a popular and functional molecular imaging technology in that it is a safe and non-invasive way. It makes use of compounds labeled with positron-emitting radioisotopes as molecular probes to image and measure biochemical processes of mammalian biology in vivo Toga and Mazziotta [2002]. Once the radiopharmaceutical is injected or inhaled, it is transported and taken up by the tissue of interest. When the positron emitted by the radiopharmaceutical meets a free electron in the tissue, their annihilation will produce two gamma ray photons traveling in opposite direction along a straight line path. If these two photons are detected within the coincidence timing window, an event is recorded along the line of response. The data summing up all of coincidence events is usually referred as a projection or sinograms, which reflects the radioisotope distribution in a way. It shows the metabolism of the tissue further and can be applied in a diagnose of the object with normal shape but abnormal functional. PET thus plays an important role in early detection and therapy of cancer. However, there are actually many pseudo-coincidences such as scattered coincidences, the random coincidences and some else. The goal of the PET image reconstruction is to reappear or estimate the radioisotope distribution in the tissue with the aid of sinogram.

There has been developed two different algorithms in past 20 years. One is so-called analytic reconstruction based on Center Section Theorem and Radon transformation. They establish the link between the sinogram and the radioisotope distribution. The analytic reconstruction often generates a poor image although it is fast and easy to use Barrett and Swindell [1996], Ollinger and Fessler [1997], which stems from that the sinogram covers lots of pseudo-coincidences besides true ones. It forces another algorithm, the iterative reconstruction. It starts out with the statistical iterative reconstruction such as ML-EM method, least square method, weighted least square method, successive over-relaxation method, etc. Shepp and Vardi [1982], Fessler [1994], Fessler [2000], Panin et al. [2006]. The statistical iteration algorithm improves the variance of the image because it takes the statistics and statistical model of the data in sinogram into account. Obviously, the statistical iteration depends on the statistical model heavily. Please refer to Leahy and Qi [2000] for an relative comprehensive review on the statistical iteration algorithm before 2002. Different from the statistical iteration, iterative algorithm in the state-space framework begins with modeling the photon arrival process in the PET system as a noisy measurement, where the state is static or dynamic radioisotope distribution Tian et al. [2004]. The latter is always associated with the compartment model and some physiological parameters Gunn et al. [2002]. The State-space model makes the iterative reconstruction based on Kalman filtering, H_∞ filtering, particle filtering possible Liu et al. [2005], Liu et al. [2012], Yu et al. [2012]. However, in order to remove the random coincidences, the delaying coincidence timing window is applied by most of PET systems. It corrupts the raw Poisson statistics, which results in a difficulty obtaining the statistics of the noises to apply Kalman filtering to reconstruct image. In spite of no need of the statistics of the noise, H_∞ filtering reconstruction is often conservative since it only takes advantage of the boundedness of the noises and neglects some noise information available.

The paper will deal with the PET reconstruction in state-space. Instead of the aforementioned filtering reconstruction, we make the most of all the information upon the noises, not only boundedness but also statistics. Lots of experiments can provide the proportion of the random coincidences eliminated by delaying coincidence window. Taken the rest of the coincidences and the eliminated coincident as two independent Poisson processes, now the statistics of the noise can be found roughly. To rule out the disadvantage from imprecise statistics, we will impose a H_∞-type constraint on the optimal reconstruction per-

⋆ This work is supported by the National Natural Science Foundation from China (under grant 61203045).

formance. In a word, the paper can provide a different algorithm. It leads to a reconstruction result which is not only close to the Kalman reconstruction as much as possible but also satisfies the H_∞ constraint.

The organization of the paper is as follows. The PET reconstruction problem are reformulated in the following section. Section III presents the solution to the reconstruction problem. Numerical experiments are given in Section III. Some conclusion remarks is made in Section IV.

Notations I is the identity matrix with the suitable dimension. For any vectors x, y, $col\{x, y\}$ means a column vector stacked by vectors x, y. For a positive definite matrix M and a vector x, $||x||_M = x'Mx$. $||x||$ denotes 2-norm of vector x. $diag\{m_1, \cdots, m_n\}$ represents a block diagonal matrix with the main diagonal matrices $m_1, \cdots, m_n$.

2. PROBLEM REFORMULATION

The main object of the paper is to reconstruct the radioisotope distribution x from the measurement y, namely, photon counting. From Tian et al. [2004], the emitting-scanning in PET system can be characterizes as

$$y = Dx + w, \tag{1}$$

where $y = \{y_i | i = 1, \cdots, M\}$ represents the sinogram data removed part of noise by the delay coincident window method. y_i means the total coincidences of the ith detector bin and M is the number of the detector bins. $x = \{x_j | i = j, \cdots, N\}$ denotes the radioisotope distribution. x_j indicates the concentration at voxel j and N is the number of the voxels one interests. D is $M \times N$ and reflects the relationship between the sinogram data and the radioisotope distribution. w is the additional noise. Assume the radioisotope distribution is time variant, then the measurement (1) at t instant can be rewritten as

$$y(t) = D(t)x(t) + w(t). \tag{2}$$

To discuss the metabolism of organism quantitatively, compartment model Gunn et al. [2002] is introduced to describe the radioisotope distribution as follows

$$\dot{x}(t) = Ax(t) + Bu(t), \tag{3}$$

where A are related to the transfer rate of the radioisotope between compartments. B is the transfer coefficient of the radioisotope from blood to tissue. $u(t)$ is the injected before PET scans.

Without loss of generality, consider the discrete-time counterpart of (3)

$$x(t+1) = Ax(t) + Bu(t). \tag{4}$$

For we interests the static radioisotope distribution, (4) becomes

$$x(t+1) = x(t). \tag{5}$$

There is no absolutely static, so a noise term is added to system (5) so that

$$x(t+1) = x(t) + v(t). \tag{6}$$

Assume $v(t)$ and $w(t)$ are mutually independent white noises with

$$E[v(t)] = 0, E[v(t)^2] = Q(t) \tag{7}$$

$$E[w(t)] = 0, E[w(t)^2] = R(t) \tag{8}$$

Meanwhile, assume they are bounded energy signals.

Remark 1. The raw counting process in the PET system is a Poisson process. Traditionally, it is recognized that pre-correcting the random coincidence via the delaying coincidence window does correct the data in mean but leads to the increased variance Leahy and Qi [2000]. Yet if one takes the eliminated photons arrival and the rest ones as two mutually independent Poisson processes, then the previous problem disappears. The data is corrected in both mean and variance. It means that one can get the statistics of the data and transform the Poisson data into the Gaussian Anscombe [1948].

Remark 2. Lots of experiments can provide the good proportion range of the random coincidences to the total coincidences. Hence, one can obtain the statistics range of the data although not guaranteeing that the statistics of data are always accurate.

Remark 1 shows that the reconstruction results based on only the H_∞ filtering may be conservative while Remark 2 shows that the reconstruction results based on only the Kalman filtering may lead to a poor results when Kalman filtering reconstruction is sensitive to the noise statistics.

In order to avoid a poor reconstruction result caused by a pure single filtering, the following constrained problem is proposed.

$$\min_{\hat{x}(t|t)} ||\hat{x}(t|t) - \hat{x}_1(t|t)||, \tag{9}$$

$$s.t. J(t+1) \geq 0, \tag{10}$$

where $\hat{x}_1(t|t)$ and $\hat{x}_2(t|t)$ are the Kalman filter and the center H_∞ filter for (6) and (2), respectively.

$$J(t) \tag{11}$$
$$= \sum_{i=0}^{t-1} \begin{bmatrix} y(i) - D(i)\hat{x}_2(i) \\ \hat{x}(i|i) - \hat{x}_2(i) \end{bmatrix}' \bar{R}(i)^{-1} \begin{bmatrix} y(i) - D(i)\hat{x}_2(i) \\ \hat{x}(i|i) - \hat{x}_2(i) \end{bmatrix}$$

is a variant of the typical H_∞ performance

$$\frac{||x(t) - \hat{x}_2(t)||^2}{||x(0) - \hat{x}(0)||^2 + ||v(t)||^2 + ||w(t)||^2} \leq \gamma^2 \tag{12}$$

along with the attenuation level γ and in finite horizon $[0, t]$, $J(0) = 0$, and $\bar{R}(i)$ will be specified in the next section.

So far, the radioisotope distribution reconstruction from the PET system is converted into an estimation problem over (6) and (2).

3. RECONSTRUCTION RESULTS

After an analysis over the noises, the PET reconstruction problem is restated as a constrained optimal filtering problem in the last section. What follows is to derive the solution to the problem.

Since the problem (9)-(10) involves those related to Kalman filtering and H_∞ filtering, we will start with providing these two filtering in form of lemmas in the following.

Lemma 1. Consider (6) and (2). The Kalman filter $\hat{x}_1(t|t)$ is given as

$$\hat{x}_1(t|t) = \hat{x}_1(t) + K_1(t)e_1(t) \tag{13}$$

where

$$e_1(t) = y(t) - D(t)\hat{x}_1(t) \tag{14}$$
$$\hat{x}_1(t+1) = \hat{x}_1(t) + K_1(t)e_1(t), \hat{x}_1(0) = 0 \tag{15}$$
$$K_1(t) = P_1(t)D(t)'M_1(t)^{-1} \tag{16}$$
$$M_1(t) = D(t)P_1(t)D(t)' + R(t) \tag{17}$$
$$P_1(t+1) = P_1(t) - K_1(t)M_1(t)K_1(t)' + Q(t), P_1(0) = 0. \tag{18}$$

Proof From Theorem 3.3.1 Hassibi et al. [1999], the proof is straightforward and is omitted.

Lemma 2. For a prescribed $\gamma > 0$, consider (6), (2) and (12). The H_∞ filtering problem is solvable if and only if Riccati equation

$$P_2(t+1) = P_2(t) - P_2(t)[D(t)'\ I]\bar{R}(t)^{-1} [D(t)'\ I]'P_2(t) + I, P_2(0) = 0 \tag{19}$$

with

$$\bar{R}(t) = \begin{bmatrix} M_2(t) & D(t)'P_2(t) \\ P_2(t)D(t) & P_2(t) - \gamma^2 I \end{bmatrix} \tag{20}$$
$$K_2(t) = P_2(t)D(t)'M_2(t)^{-1} \tag{21}$$
$$M_2(t) = D(t)P_2(t)D(t)' + I \tag{22}$$

has a positive semi-definite solution such that $\bar{R}(t)$ and $diag\{I, -I\}$ have the same inertia. Moreover, the H_∞ center filter $\hat{x}_2(t|t)$ can be given as

$$\hat{x}_2(t|t) = \hat{x}_2(t) + K_2(t)e_2(t) \tag{23}$$

where

$$e_2(t) = y(t) - D(t)\hat{x}_2(t) \tag{24}$$
$$\hat{x}_2(t+1) = \hat{x}_2(t) + K_2(t)e_2(t), \hat{x}_2(0) = 0. \tag{25}$$

Proof From Lemma 4.3.3 Hassibi et al. [1999], the proof is straightforward and is omitted.

Now we at a position provide the solution to the problem (9) subject to (10).

Theorem 1. For a prescribed $\gamma > 0$, consider (6),(2) and (9)-(10). Then the optimal $\hat{x}(t|t)$ can be given as

$$\hat{x}(t|t) = \begin{cases} \hat{x}_1(t|t), if\ \hat{x}_1(t|t)\ satisfies\ (10); \\ \theta\hat{x}_1(t|t) + (1-\theta)\hat{x}_2(t|t), otherwise. \end{cases} \tag{26}$$

where $\theta \in (0, 1)$ and is given as

$$\theta = \frac{a(t)^{1/2}}{||\hat{x}_1(t) - \hat{x}_2(t)||_{b(t)}} \tag{27}$$

with

$$a(t) = J(t) + e_2(t)'M_2^{-1}(t)e_2(t) \tag{28}$$
$$b(t) = [\gamma^2 I - (P_2^{-1}(t) + D(t)'D(t))^{-1}]^{-1}. \tag{29}$$

Proof It is not hard that (9)-(10) is convex. According to Kuhn-Tucker condition, the solution $\hat{x}(t|t)$ should satisfy the following equation system

$$\hat{x}(t|t) - \hat{x}_1(t|t) + \lambda(\hat{x}(t|t) - \hat{x}_2(t|t)) = 0, \tag{30}$$
$$\lambda \geq 0, \tag{31}$$
$$\lambda[a(t) - (\hat{x}(t|t) - \hat{x}_2(t|t))'b(t)(\hat{x}(t|t) - \hat{x}_2(t|t))] = 0, \tag{32}$$

where λ is the relaxation factor. One can solve them in three cases.

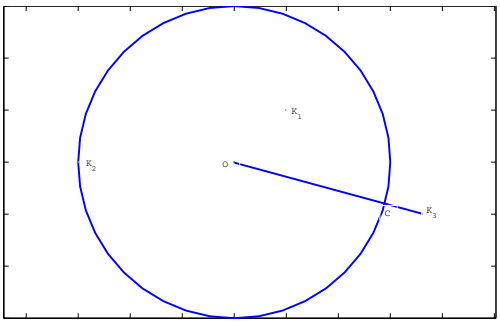

Fig. 1. the link between the unconstrained solution $\hat{x}_1(t|t)$ and the feasible region $B(O, a(t)^{1/2})$

Case I.

$$\begin{cases} \lambda = 0 \\ J(t+1) \neq 0 \end{cases} \tag{33}$$

which implies that $\hat{x}_1(t|t)$ is just located inside feasible region as K_1 in Fig.1. Hence, the constrained problem is converted into a optimal one without constraint and it is straightforward that $\hat{x}(t|t) = \hat{x}_1(t|t)$.

Case II.

$$\begin{cases} \lambda = 0 \\ J(t+1) = 0 \end{cases} \tag{34}$$

which implies that $\hat{x}_1(t|t)$ is just located in the boundary of the feasible region as K_2 in Fig 1. Hence, there still holds $\hat{x}(t|t) = \hat{x}_1(t|t)$.

Case III.

$$\begin{cases} \lambda > 0 \\ J(t+1) = 0 \end{cases} \tag{35}$$

which means $\hat{x}_1(t|t)$ is outside the feasible region as K_3 in Fig.1. Hence, the optimal solution should be located in the boundary of the feasible region. It is not easy to solve λ directly, so we handle the problem from geometrical view. Let $||z||_{b(t)} = (z'b(t)z)^{1/2}$, which virtually define a norm by virtue of the inertia condition in Lemma 2. Now the feasible region is in fact a closed ball with center $\hat{x}_2(t|t)$ and radius $a(t)^{1/2}$, see Fig.1. Hence, the potential optimal solution $\hat{x}(t|t)$ should be the point C where the ball $B(O, a(t)^{1/2})$ and the line K_3O cross, i.e. $\theta\hat{x}_1(t|t) + (1-\theta)\hat{x}_2(t|t)$. For verify that point C is the optimal solution, one still needs to prove $\lambda > 0$. From (32), there holds

$$\lambda = -\frac{[\hat{x}(t|t) - \hat{x}_2(t|t)]'[\hat{x}(t|t) - \hat{x}_1(t|t)]}{||[\hat{x}(t|t) - \hat{x}_2(t|t)]||^2}. \quad (36)$$

Denote α as the angle between the vector $\hat{x}(t|t) - \hat{x}_2(t|t)$ and vector $\hat{x}(t|t) - \hat{x}_1(t|t)$, it is clear that $\alpha = \pi$. Now one has $\lambda = ||\hat{x}(t|t) - \hat{x}_1(t|t)||/||\hat{x}(t|t) - \hat{x}_2(t|t)|| > 0$ from $cos(\alpha) = -1$. The proof is completed.

It is shown by Theorem 1 that the Kalman filter is the optimal one among all of H_∞ filters when the Kalman filter is located inside the H_∞ constrained region; Otherwise, the optimal one is the H_∞ filter located in the boundary of the H_∞ constrained region and nearest to the Kalman filter.

Remark 3. Although Theorem 1 is proposed for the static image reconstruction, it is suitable for the dynamic image reconstruction. It is should be stressed that the idea achieving a performance subject to another performance can lead to a practical results.

4. NUMERICAL EXPERIMENTS

The reconstruction method in the paper is validated with the computer-synthesized Zubal-thorax-phantom.

The true Zubal-thorax-phantom and its sinogram are shown in Fig. 2 and Fig. 3, respectively.

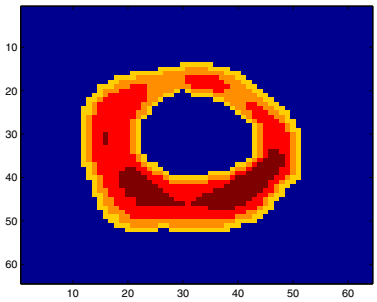

Fig. 2. the ture Zubal-thorax-phantom

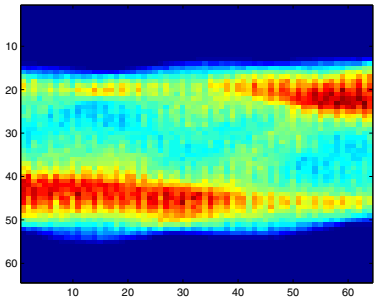

Fig. 3. Sinogram

For comparing the reconstruction performance in the paper, the Kalman filtering (KF) reconstruction, H_∞ filtering (HF) reconstruction and the constrained filtering (CF) reconstruction algorithm proposed in the paper are applied to two different noise parameters. Parameters I match the noises well and can guarantee that the Klaman reconstruction recovers the Zubal-thorax-phantom better than parameters II unmatched with the noise level. The reconstruction results of 3 algorithms for parameters I are displayed in Fig. 4, Fig. 5 and Fig. 6, respectively. The reconstruction results of 3 algorithms for parameter II are shown in Fig. 7, Fig. 5, and Fig. 8, respectively. Different from the performance of the pure single filtering reconstruction algorithm, KF or HF algorithm, it is clear that CF algorithm can leads to a nice image reconstructions whether the statistics matches the noises level or not. Or rather, the CF algorithm is more suitable than the KF and HF algorithms since one does not know whether the statistics matches the noise level in advance.

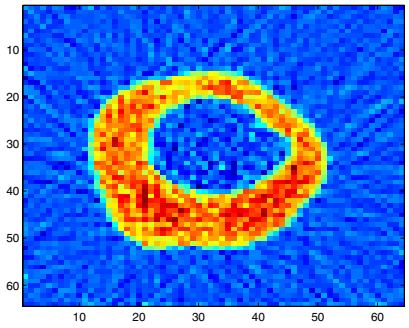

Fig. 4. Reconstructed image: KF at matched noise level

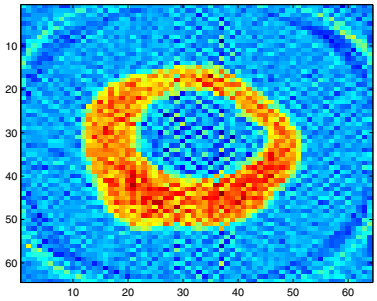

Fig. 5. Reconstructed image: HF at matched noise level

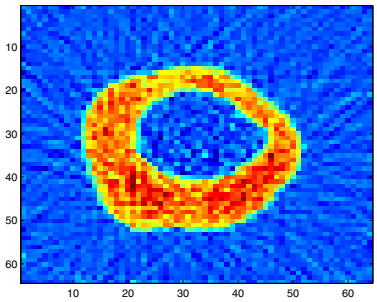

Fig. 6. Reconstructed image: CF at matched noise level

We can also compare the reconstruction results via the error $bias = \frac{1}{N}\sum_{i=1}^{N}(x_i - \hat{x}_i)$ and $variance = [\frac{1}{N-1}\sum_{i=1}^{N}(x_i - \hat{x}_i)^2]^{1/2}$, see Table 1 as follows. Table 1 shows that the CF algorithm may not present the best

one of the 3 reconstruction results, yet it is the best one when one does not know whether the statistics matches the noise level or not in advance.

5. CONCLUSION

The paper provides a new algorithm of image reconstruction for PET systems. Different from the Kalman or H_∞ algorithm, the algorithm in the paper can guarantee the quality of reconstructed image whether the statistics of noises is accurate enough or not. If the statistics is relatively accurate, the reconstruction result is provided based on the Kalman filtering; otherwise, the reconstruction result is given based on the H_∞ filter nearest to the Kalman filter.

REFERENCES

Anscombe, F.J. (1948). The transformation of poisson, binomial and negative-binomial data. *Biometrika*, 35(3/4), 246–254.

Barrett, H.H. and Swindell, W. (1996). *Radiological imaging: the theory of image formation, detection, and processing*. Academic Press.

Fessler, J.A. (1994). Penalized weighted least-squares image reconstruction for positron emission tomography. *Medical Imaging, IEEE Transactions on*, 13(2), 290–300.

Fessler, J.A. (2000). Statistical image reconstruction methods for transmission tomography. *Handbook of Medical Imaging*, 2, 1–70.

Gunn, R., Gunn, S., Turkheimer, F., Aston, J., and Cunningham, V. (2002). Tracer kinetic modeling via basis pursuit. *Academic*, 115–121.

Hassibi, B., Sayed, A., and Kailath, T. (1999). *Indefinite-Quadratic Estimation and Control: A Unified Approach to H_2 and H_∞ Theories*. Society for Industrial Mathematics.

Leahy, R.M. and Qi, J. (2000). Statistical approaches in quantitative positron emission tomography. *Statistics and Computing*, 10(2), 147–165.

Liu, H., Tian, Y., and Shi, P. (2005). Pet image reconstruction: A robust state space approach. In *Information Processing in Medical Imaging*, 197–209. Springer.

Liu, H., Wang, S., Gao, F., Tian, Y., Chen, W., Hu, Z., and Shi, P. (2012). Robust framework for pet image reconstruction incorporating system and measurement uncertainties. *PloS one*, 7(3), e32224.

Ollinger, J.M. and Fessler, J.A. (1997). Positron-emission tomography. *Signal Processing Magazine, IEEE*, 14(1), 43–55.

Panin, V., Kehren, F., Rothfuss, H., Hu, D., Michel, C., and Casey, M. (2006). Pet reconstruction with system matrix derived from point source measurements. *Nuclear Science, IEEE Transactions on*, 53(1), 152–159.

Shepp, L.A. and Vardi, Y. (1982). Maximum likelihood reconstruction for emission tomography. *Medical Imaging, IEEE Transactions on*, 1(2), 113–122.

Tian, Y., Liu, H., and Shi, P. (2004). State space strategies for estimation of activity map in pet imaging. In *Medical Imaging and Augmented Reality*, 46–53. Springer.

Toga, A. and Mazziotta, J. (2002). *Brain Mapping: The Methods*. Brain mapping : the method (2nd edition). Academic Press.

Yu, F., Liu, H., and Shi, P. (2012). Pet image reconstruction based on particle filter framework. In *Biomedical and Health Informatics (BHI), 2012 IEEE-EMBS International Conference on*, 851–853.

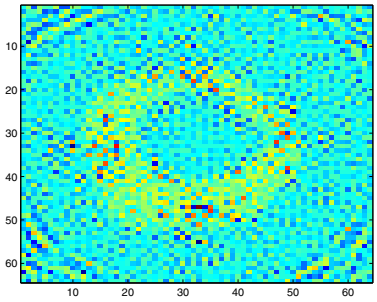

Fig. 7. Reconstructed image: KF at unmatched noise level

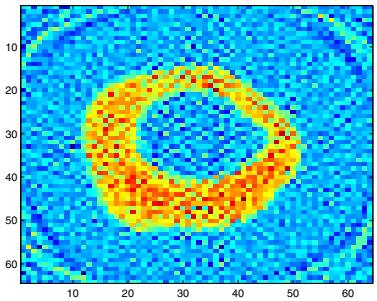

Fig. 8. Reconstructed image: CF at unmatched noise level

Table 1. Bias and Variance of Each Method

statistics	algorithm	bias ± variance
at matched noise level	KF	-0.0004954± 4.1984
	HF	-0.0004953± 4.2593
	CF	-0.0004954± 4.1984
at unmatched noise level	KF	-0.0004956± 5.9292
	HF	-0.0004953± 4.2593
	CF	-0.0004954± 4.2979